batteries

MDPI

Article

An Experimental Study of Power Smoothing Methods to Reduce Renewable Sources Fluctuations Using Supercapacitors and Lithium-Ion Batteries

Dario Benavides [1,2], Paul Arévalo [2,3], Marcos Tostado-Véliz [3,*], David Vera [3], Antonio Escamez [3], José A. Aguado [1] and Francisco Jurado [3]

[1] Department of Electrical Engineering, Smart Campus, University of Malaga, 29010 Malaga, Spain
[2] Department of Electrical, Electronics and Telecommunications Engineering (DEET), Balzay Campus, University of Cuenca, Cuenca 010107, Ecuador
[3] Department of Electrical Engineering, University of Jaen, 23700 Linares, Spain
* Correspondence: mtostado@ujaen.es

Abstract: The random nature of renewable sources causes power fluctuations affecting the stability in the utility grid. This problem has motivated the development of new power smoothing techniques using supercapacitors and batteries. However, experimental studies based on multiple renewable sources (photovoltaic, wind, hydrokinetic) that demonstrate the validity of power smoothing techniques under real conditions still require further study. For this reason, this article presents a feasibility study of a renewable grid-connected system, addressing various aspects based on power quality and energy management. The first of them is related to the fluctuations produced by the stochastic characteristics of renewable sources and demand. Two power smoothing algorithms are presented (ramp rate and moving average) combining photovoltaic, wind, and hydrokinetic sources with a hybrid storage system composed of supercapacitors and lithium-ion batteries. Then, the self-consumption for an industrial load is analyzed by studying the energy flows between the hybrid renewable energy sources and the grid. The main novelty of this paper is the operability of the supercapacitor. The experimental results show that when applying the power smoothing ramp rate method, the supercapacitor operates fewer cycles with respect to the moving average method. This result is maintained by varying the capacity of the renewable sources. Moreover, by increasing the capacity of photovoltaic and wind renewable sources, the hybrid storage system requires a greater capacity only of supercapacitors, while by increasing the capacity of hydrokinetic turbines, the battery requirement increases considerably. Finally, the cost of energy and self-consumption reach maximum values by increasing the capacity of the hydrokinetic turbines and batteries.

Keywords: power smoothing; self-consumption; hydrokinetic; supercapacitor; experimental

Citation: Benavides, D.; Arévalo, P.; Tostado-Véliz, M.; Vera, D.; Escamez, A.; Aguado, J.A.; Jurado, F. An Experimental Study of Power Smoothing Methods to Reduce Renewable Sources Fluctuations Using Supercapacitors and Lithium-Ion Batteries. *Batteries* **2022**, *8*, 228. https://doi.org/10.3390/batteries8110228

Academic Editor: Joeri Van Mierlo

Received: 27 September 2022
Accepted: 5 November 2022
Published: 9 November 2022

1. Introduction

Renewable energy sources (RESs) are a potential candidate to replace fossil fuels in the long term. Their technological development in recent decades has caused a greater penetration in grid-connected systems, e.g., studies show that the photovoltaic (PV) energy capital expenditure drops to 75% by 2050 [1]. Therefore, the intensive penetration of PV energy in the utility grid causes voltage and frequency stability problems due to the variable characteristics of the solar resource [2,3]. Power peaks produced by the movement of clouds in PV systems can reach up to 60% of their installed capacity. If the PV output power is sent to the grid without any energy control system or power smoothing method, it could cause strong problems of stability and energy quality [4]. To deal with these drawbacks, some electricity supplier companies have used specific ranges of power variations of PV plants connected to the grid, e.g., in Mexico the output PV power variations must be mitigated within 1%/min to 5%/min of installed capacity and 10%/min in Puerto Rico [5].

Wind generation has evolved widely in some European countries, being able to operate in conjunction with PV and energy storage systems (ESS) [6]. However, wind turbine (WT) generator voltage fluctuations, which are caused by the turbulent nature of wind speed, present disruptions to a battery's charge controller and affect battery energy system (BES) life, similar to PV systems [7]. In this context, the integration of supercapacitors (SCs) provides smooth charging and long discharge of the BES and keeps the power electronic circuit safe from current spikes during battery charging cycles [8,9]. Power smoothing has been successfully tested even in hybrid renewable systems (HRES) with PV + WT sources [10]. In this sense, hydrokinetic turbines (HKT), less studied than PV systems, are useful for communities near rivers. The variability of the river speed is not as pronounced as in PV systems. Moreover, if the installed capacity is large, the variations of output HKT power could significantly reduce energy quality and reliability [11], especially in (PV + HKT). Therefore, the development of power smoothing strategies in PV + HKT systems on a grid are necessary.

There is extensive research in the literature on power smoothing methods in PV systems. Generally, geographical dispersion to mitigate short-term power fluctuations based on the grouping of PV plants and the distance between them has been used, where the short-term output power fluctuation of a geographically dispersed PV system is reduced compared to a single PV array [12]. When PV power plants are distributed, voltage fluctuations are greatly reduced but not eliminated. Thus, in Ref. [13], it is shown that for dispersions greater than 800 km, a small reduction in energy production is observed. For this reason, this limit must be considered in power smoothing based on the dispersion of PV systems. Some authors have proposed the integration of diesel or natural gas generators to mitigate PV fluctuations although the time it takes for these sources to respond to this sudden change is slow. Additionally, there is a decrease in operational efficiency when operating at low output power levels during a high PV swing level [14,15]. Derating PV power is a conventional method of suppressing output power fluctuations through constraints imposed by a maximum power point tracking (MPPT) controller. The smoothing effect created by limiting PV power increases to 1% of nominal capacity, as some result fluctuations can be reduced by up to 12%/min. However, this proposed method does not consider the limitation of the PV output when the radiation decreases. For this reason, the authors do not recommend this technique since limiting output power means large economic losses [16]. Another classic method to maintain voltage levels within the limits established by the electricity supply companies is through a dump load. This method consists of installing a resistive load with a controller to manage the flow of energy through the load, though this technique causes the same energy and economic problems as power curtailment using MPPT [17].

To solve the aforementioned problems, researchers have proposed several methods to reduce PV fluctuations using BES at the point of common coupling (PCC) because of their high energy density. Based on the literature review, the BES control is based on the state-of-charge (SOC) level. Lead acid batteries are inexpensive for short-term applications (2 years). Installation of sodium sulfur batteries for a period of 4 to 6 years is economical for BES applications. Lithium-ion (LI) and solid-state BES show promise through falling prices and rising performance trends [18]. Lithium-ion (LI) batteries have proven to be one of the most promising energy storage devices for applications in electric vehicles, smart grids, large-scale energy storage systems, and portable electronic devices [19]. BES avoids power curtailment. However, being subjected to fast charging/discharging cycles considerably decreases its useful life since a BESS can perform a limited number of cycles [20]. This was demonstrated in Ref. [21] through tests of SOC in LI batteries, where the depth of discharge is a determining factor. This means the increase in maintenance cost and the frequent addition of distilled water are some of the disadvantages of the BES [22].

This problem has motivated the development of methods to smooth out power fluctuations by using an SC to absorb power peaks. An SC's high power density allows it to smooth out faster power fluctuations that batteries are not capable of [23]. A combined supercapacitor and battery storage system accommodates rapid power changes, provid-

ing system stability and helping achieve power smoothing [24,25]. In addition, recent research on organometallic framework materials, such as SC electrodes, has shown promising results [26]. For example, Ref. [27] has developed a novel method to reduce power fluctuations considering PV output power curtailment. The authors combined an SC and batteries forming a hybrid energy storage system (HESS). The results show that when using an SC, the charge/discharge cycles of the BES are considerably reduced. Likewise, energy management of a microgrid composed of PV/fuel cells/BES/SC is presented. The energy control causes the BSS to operate in a SOC of 56% and 65.4% [28]. In this type of residential HESS system, the BES have relatively short lifespans and produce chemical waste; therefore, a feasibility study that demonstrates that the use of BES for applications such as power smoothing is necessary. The ramp rate-based power smoothing method allows setting fine-tuned maximum and minimum peak limits [29]. In order to clarify this point, Ref. [30] presents a suitability study of three types of energy storage systems (ESS): rechargeable batteries, electrochemical capacitors, and electrolytic capacitors. The article proposes a power smoothing method based on ramp-rate control, the results show that the ideal ESS for this type of application must have high power density and adequate energy flow control. However, the study is limited to mathematical solutions and computer simulation; a realistic environment that includes real data may behave differently from idealized simulations. Therefore, laboratory tests are needed to substantiate the proposed study for the authors. Within a residential context, Tiezohou Wu et al., [31] present an improvement of the particle swarm optimization (PSO) algorithm together with a variable filter time constant for a HESS composed of an SC and BES. The authors present results using an experimental platform. The power and SOC of the BES are analyzed. This allows data to be analyzed in real systems. Nevertheless, it is not possible to determine the accuracy of the computer models since a comparison is not made between the model and the experimental tests.

Several authors studied new methods and techniques of power smoothing using HESS, e.g., in Ref. [32] a distributed rule-based supervisory control and power management technique in a PV/HESS is presented. The case study system consists of a PV system, a load, and an HESS that contains a BES and an SC, to reduce the PV fluctuations. The authors propose a method based on an adaptive filter controlled by programmed automata. The results of the simulations show that the computational load is considerably reduced. Wei Ma et al. [5] present an analysis regarding the optimal allocation of a HESS (SC/BES) to reduce PV fluctuations. The study aims to reduce costs by optimizing the annual energy flow through a novel power smoothing method presented. Mukalu S. et al. [33] propose a hierarchical predictive control for a supercapacitor-retrofitted grid-connected HESS for a large PV plant with a BES. Similarly, Guishi W. et al. [34] discuss a power smoothing method for a large PV plant using an SC and vanadium redox flow batteries.

In the aforementioned studies, the authors focus on comparing new methods of power smoothing in PV systems using an SC and batteries. The results are based on idealized simulations; the authors do not consider real operation limits of the inverters. In addition, studies are needed to determine the voltage in PCC, the self-consumption of prosumers connected to the utility grid, the charging/discharging cycles of an SC, and the accuracy of the presented models. Although most of the literature combines SC/BES, it is possible to propose new technologies that reduce PV fluctuations together with SCs. HKTs are little investigated technologies. In Ref. [35], the stability of a PV/wave power system is analyzed. However, the behavior of the waves is different from the speed of a river in an HKT. In Ref. [35], the SCs reduce the oscillations of PV power and the power-generation system (WPGS) and do not team up to smooth the power peaks produced by the PV system. Furthermore, the energy analysis and power smoothing of the combination of several RES and HESS is relatively new.

Therefore, the proposed study of reducing the power fluctuations of a PV/WT/HKT system using LI/SC is new. After analyzing the available literature, the following research questions arise:

- Is LI/SC feasible to reduce power fluctuations of a PV/WT/HKT system?
- What power smoothing technique is recommended?
- What is the accuracy of a computational model concerning an experimental result?
- Are the voltage fluctuations in PCC within the limits established by the electricity distribution companies?
- What happens to the self-consumption of a combined multi-source system?
- What is the behavior of the charge/discharge cycles and the depth of charge of an SC in increasing the capacity of the RES?

To answer these research questions, this paper presents a comparison of two power smoothing methods for a grid-connected PV/WT/HKT system and an industrial load demand. Exhaustive simulations and laboratory experiments are carried out to decide the feasibility of the proposed system. The methods and techniques of power smoothing are extensive in the literature. Based on studies, two techniques have been chosen that are mostly used for this study, moving average and ramp-rate [36,37]. In summary, to fill the gaps in the available literature, the main contributions of this paper are:

- Comparison of two power smoothing methods for a grid-connected PV/WT/HKT/Load system using LI/SC is performed.
- Sensitivity analysis based on self-consumption and power smoothing response in PCC is performed.
- Study of the daily energy cost of the HRES adding a WT, an HKT, and LI batteries.
- Determination of the error between experimental tests and computer simulations.
- Combination study between the proposed RES and ESS.

The remainder of the paper is organized as follows. Section 2 presents the background, where the methodology and the input variables are present. Section 3 shows the mathematical modeling. Then, in Section 4, energy management and power smoothing algorithm are explained. Section 5 discusses the results obtained from the experiment. These have been classified according to power smoothing, cost, self-consumption, and sensitivity analysis. Finally, Section 6 concludes the paper.

2. Background

The proposed methodology is summarized in the flowchart of Figure 1. Firstly, real data are considered for mathematical modeling representing the physical and electrical characteristics of the components of the hybrid renewable system (HRES). Computer simulations aim to demonstrate the validity of experimental results in the laboratory. Then, two well-known power smoothing algorithms (MA and RR) are compared, progressively adding various renewable sources and energy storage systems. This procedure allows various sensitivity analyses based on technical and economic indices that are shown in the results of this paper.

The topology of the proposed HRES is shown in Figure 2. The EMS system controls the PV, SC, HKT, WT, and LI circuit breakers. The PCC is the point where energy flows to/from the utility grid. Power smoothing methods and energy control allow for an improved power flow at the PCC point.

The input variables are made up of renewable resources in the study area. In this case, real data of solar radiation, wind speed, and ambient temperature have been taken from a weather station. The demand data have been measured from a factory located in the city of Cuenca. The shifted peaks and the river speed are measured by a hydrological station located south of Ecuador. Figure 3 shows the behavior of the input data for a random day. Intermittent power sources such as the PV system and the WT generate high fluctuations in the electrical grid. For this reason, it is important to consider what its mitigation with rapid-response ESS means. On the other hand, the river speed does not present a higher rate of change with respect to time. However, this resource is not available throughout the year and requires robust ESS to optimize its management with the required demand.

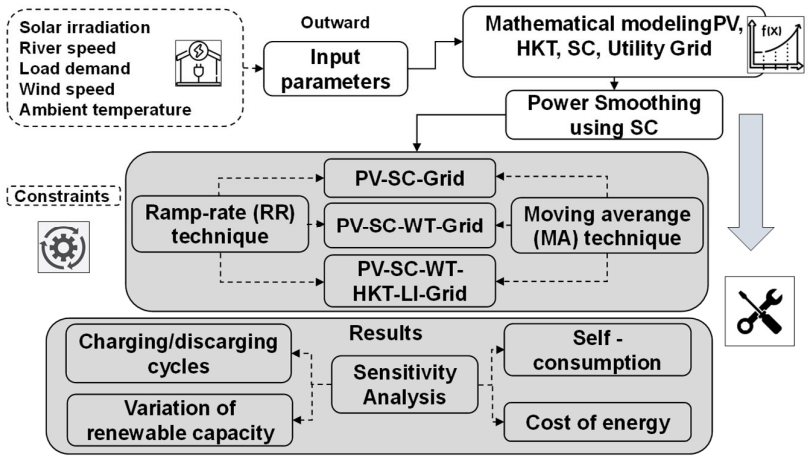

Figure 1. Flowchart of the proposed methodology.

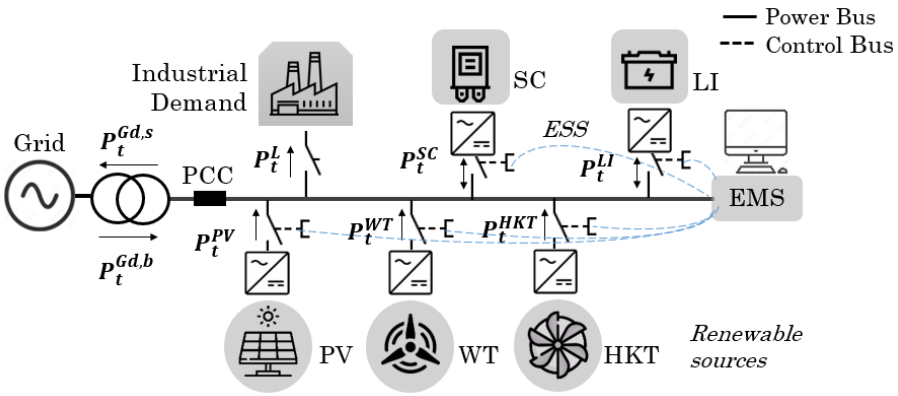

Figure 2. System topology and information flows of PV-HKT-WT-LI-Grid-Load demand and SC.

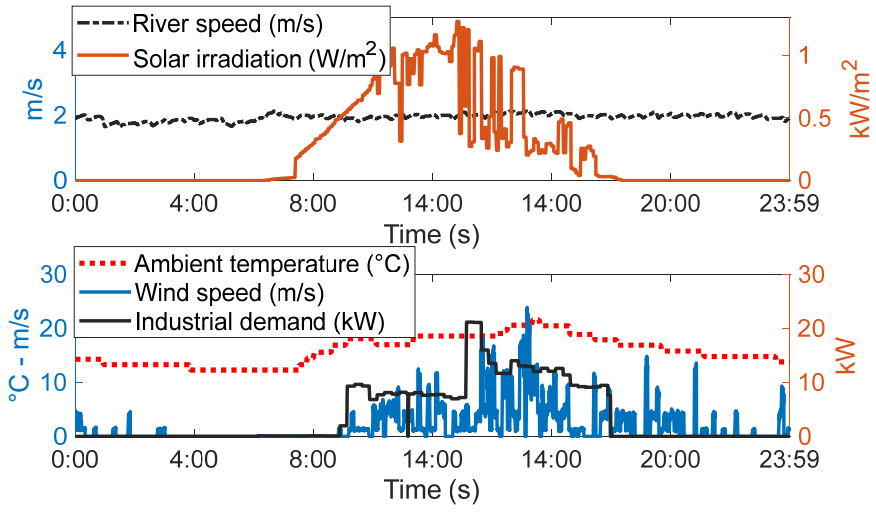

Figure 3. Input parameters, time interval: average values every second during a day.

3. Mathematical Modeling

3.1. Photovoltaic Model

The electrical output power (P_t^{PV}) of the PV system is calculated with Equation (1) [38]:

$$P_t^{PV} = \gamma_t^{PV}.\lambda^{PV}.\left(\frac{I_{T,t}^{PV}}{I_{S,t}^{PV}}\right).\left[1+\alpha_{pw}^{PV}.\left(T_C^{PV}-T_S^{PV}\right)\right]; \forall t \in T \cup \Xi \quad (1)$$

where γ_t^{PV} is the rated capacity of the photovoltaic, λ^{PV} is the electrical output power of PV, $I_{T,t}^{PV}$ is the photovoltaic current generated by the incident radiation in the cell, $I_{S,t}^{PV}$ is the reverse saturation diode current, α_{pw}^{PV} is the temperature power coefficient, T_C^{PV} is the cell temperature in the photovoltaic array, T_S^{PV} is the cell temperature under standard test conditions, T is the number of time intervals, and Ξ is the set of the power smoothing methods.

To avoid a negative power output flow, Equation (2) must be satisfied:

$$1 + \alpha_{pw}^{PV}.\left(T_C^{PV} - T_S^{PV}\right) \geq 0;\ \text{if } \left|I_{T,t}^{PV}\right| \text{ and } \left|I_{S,t}^{PV}\right| \tag{2}$$

Moreover, to avoid indeterminacy, in Equation (2) $I_{S,t}^{PV} \neq 0; \forall t \in T \cup \Xi$. The values of the coefficients related to this mathematical model have been taken from the real photovoltaic system in the Microgrid Laboratory of the University of Cuenca, details shown in Ref. [39].

3.2. Hydrokinetic Turbine Model

The electrical output power $\left(P_t^{HKT}\right)$ of the HKT system is calculated with Equation (3) [40]:

$$P_t^{HKT} = \begin{cases} \frac{1}{2}.\rho^{\omega}.A^{HKT}.\alpha_{HKT,t}^3.\zeta_p^{HKT}.\eta^{HKT} & \text{if } \alpha_{HKT} \geq \alpha_{HKT,\,cut-in} \\ 0 & \text{if } \alpha_{HKT} < \alpha_{HKT,\,cut-in} \\ P_t^{HKTmax} & \text{if } \alpha_{HKT} < \alpha_{HKT,\,cut-off} \end{cases} \quad \forall t \in T \cup \Xi \tag{3}$$

where ρ^{ω} is water density, A^{HKT} is the HKT turbine sweep surface, $\alpha_{HKT,t}$ is the river speed, ζ_p^{HKT} is the HKT power coefficient, η^{HKT} is the HKT efficiency, and P_t^{HKTmax} is the maximum power of the HKT. The power coefficient in the HKT has values of approximately 0.4, subject to the Betz limit of 59.3%. Therefore, an energy limit is constrained, $P_{c,t}^{HKT} \leq P_t^{HKTmax}$ [40]. The values of the coefficients related to this mathematical model have been taken from the real hydrokinetic turbine in the Microgrid Laboratory of the University of Cuenca, details shown in Ref. [39].

3.3. Wind Turbine Model

The mathematical representation of a wind turbine is similar to that of an HKT. The output power of the WT (P_t^{WT}) is shown in Equation (4) [41]:

$$P_t^{WT} = \frac{1}{2}.\rho^{air}.A^{WT}.V_{WT,t}^3.C_p^{WT}(\varsigma,\ \beta);\ \forall t \in T \cup \Xi \tag{4}$$

where ρ^{air} is air density, A^{WT} is the wind turbine sweep surface, $V_{WT,\,t}$ is the wind speed, and C_p^{WT} is the wind turbine power coefficient. The power coefficient is expressed with Equation (5) [41]:

$$C_p^{WT}(\varsigma,\ \beta) = \frac{1}{2}\left[\frac{116}{\varsigma_i} - (0.4).\beta - 5\right]e^{\frac{-21}{\varsigma_i}} \tag{5}$$

where ς is the tip-speed ratio, and β is the blade pitch angle; ς_i and ς are given, respectively, by Equations (6) and (7):

$$\varsigma_i = \left[\frac{1}{\varsigma + (0.08).\beta} - \frac{0.035}{\beta^3}\right]^{-1} \tag{6}$$

$$\varsigma = \frac{\Omega_t.R}{V};\ \forall t \in T \cup \Xi \tag{7}$$

where Ω_t is the turbine rotor speed. The Betz coefficient suggests that a WT can extract a maximum of 59.3% of the energy in an undisturbed wind current. The values of the coefficients related to this mathematical model have been taken from the real wind turbine in the Microgrid Laboratory of the University of Cuenca, details shown in Ref. [39].

3.4. Supercapacitor Model

The energy available in the SC depends on their capacitance value and the operating voltage range of the inverter. The energy of an SC (E_t^{SC}) at any time (t) is calculated with Equation (8) [40]:

$$E_t^{SC} = \frac{1}{2}.C^{SC}.(V_{max,\,t}^{SC} - V_{min,\,t}^{SC})^2; \forall t \in T \cup \Xi \quad (8)$$

where C^{SC} is the capacitance of the SC, $V_{max,\,t}^{SC}$ is the SC voltage upper, and $V_{min,\,t}^{SC}$ is the SC voltage lower limit.

Power smoothing techniques require control over the SOC of the SC; thus, this parameter is represented by Equation (9):

$$SOC_t^{SC} = \frac{V_t^{SC} - V_{min,\,t}^{SC}}{V_{max,\,t}^{SC} - V_{min,\,t}^{SC}}; \forall t \in T \cup \Xi \quad (9)$$

Under normal conditions, the nominal voltage and current values must be kept within the operating limits of the inverter. Equations (10) and (11) show the SC constraints:

$$V_{min,\,t}^{SC} < V_t^{SC} < V_{max,\,t}^{SC}; \forall t \in T \cup \Xi \quad (10)$$

$$I_t^{Ch,max} < I_t^{SC} < I_t^{Dis,max}; \forall t \in T \cup \Xi \quad (11)$$

where I_t^{SC} is the nominal current in the SC, $I_t^{Ch,max}$ is the maximum charge current allowed in the SC, and $I_t^{Dis,max}$ is the maximum discharge current allowed in the SC. The values of the coefficients related to this mathematical model have been taken from the real supercapacitors bank in the Microgrid Laboratory of the University of Cuenca, details shown in Ref. [39].

3.5. Lithium-Ion Battery Model

The state of charge of lithium-ion batteries during the charging process (k + 1) can be expressed with Equation (12) [33]:

$$SOC_t^{LI}(k+1) = SOC_t^{LI}(k) + \eta_{inv}.\eta_{LI}^{ch}.P_t^{LI+}(k+1).\Delta T - \frac{1}{\eta_{inv}.\eta_{LI}^{d}} P_t^{LI-}(k+1).\Delta T \quad (12)$$

where η_{inv} is the efficiency of the inverter that connects the battery to the grid, η_{LI}^{ch} is the battery efficiency during the charging process, $P_t^{LI+}(k+1)$ is the output power of the battery during the charge process (k + 1), $P_t^{LI-}(k+1)$ is the output power of the battery during the discharge process (k + 1), η_{LI}^{d} is the battery efficiency during the discharging process, and ΔT is time interval under analysis. The state of charge (SOC) of the battery for any time is limited by Equations (13)–(15):

$$\underline{SOC_t^{LI}} < SOC_t^{LI}(k) < \overline{SOC_t^{LI}}, \forall t \in T \cup \Xi \quad (13)$$

$$0 \leq P_t^{LI+}(k) < \frac{\overline{P_{LI}^{ch}}}{\eta_{inv}}, \forall t \in T \cup \Xi \quad (14)$$

$$0 \leq P_t^{LI-}(k) < \eta_{inv}/\overline{P_{LI}^{disch}}, \forall t \in T \cup \Xi \quad (15)$$

where SOC_t^{LI} is the lower bound state of charge in an LI battery at time t, $\overline{SOC_t^{LI}}$ is the lower bound state of charge in the LI battery at time t, $P_t^{LI+}(k)$ is the output power of the battery bank at time t (kW) during (k) the charging process, $\overline{P_{LI}^{ch}}$ is the upper bound charging power, P_t^{LI-} is the output power of the battery bank at time t (kW) during (k) the discharging

process, and $\overline{P_{LI}^{disch}}$ is the lower bound discharging power. Equations (16) and (17) prevent the simultaneous charging and discharging of batteries:

$$P_t^{LI+}(k) \cdot P_t^{LI-} = 0; \forall t \in T \cup \Xi \quad (16)$$

$$P_t^{LI} = P_t^{LI-}(k) - P_t^{LI+}; \forall t \in T \cup \Xi \quad (17)$$

The values of the coefficients related to this mathematical model have been taken from the real lithium-ion battery bank in the Microgrid Laboratory of the University of Cuenca, details shown in Ref. [39].

It is important to mention that the performance of the lithium-ion battery depends mainly on the collective impact of the discharge current and the ambient temperature [42]. Therefore, to avoid a very high current discharge, the hybrid system combined with supercapacitors that absorb high fluctuations and smooth the reference power to the batteries has been proposed. This proposal avoids an excessive number of battery charge and discharge cycles and keeps the depth of discharge at an adequate percentage. However, the scope of this paper does not include battery performance studies, and the ambient temperature is between 8 °C to 20 °C, which does not imply a problem.

3.6. Utility Grid Model

The power flow is bidirectional with respect to the utility grid. It is assumed that the power system is an infinite bus connected in parallel to the HRES. The power restrictions from/to the grid depend on the capacity of the transmission lines, transformer, and the electricity distribution company. These restrictions are expressed in Equations (18) and (19) [9]:

$$0 \leq P_t^{Gd,b} \leq \tau_t^{Gd,b} \overline{p_t^{Gd,b}}; \forall t \in T \cup \Xi \quad (18)$$

$$0 \leq P_t^{Gd,s} \leq \tau_t^{Gd,s} \overline{p_t^{Gd,s}}; \forall t \in T \cup \Xi \quad (19)$$

where $P_t^{Gd,b}$ is the power from the grid to users, $\tau_t^{Gd,b}$ is a binary variable which is equal to one if the grid supplies to users, $\overline{p_t^{Gd,b}}$ is the maximum transmittable power from the grid to users, $P_t^{Gd,s}$ is surplus electricity sent to the grid, $\tau_t^{Gd,s}$ is a binary variable equal to one if the surplus electricity is sent to the grid, and $\overline{p_t^{Gd,s}}$ is the maximum transmittable surplus electricity to the grid. Then, the power flow between the HRES and the utility grid can have only one direction; therefore:

$$\tau_{c,t}^{Gd,b} + \tau_{c,t}^{Gd,s} \leq 1; \forall t \in T \cup \Xi \quad (20)$$

Likewise, in case of power outages due to external faults, the power flow between the HRES and the utility grid must be restricted by means of circuit breakers. These constraints are expressed in Equations (21) and (22):

$$\tau_t^{Gd,b} = O; \forall t \in T \cup \Xi \quad (21)$$

$$\tau_t^{Gd,s} = O; \forall t \in T \cup \Xi \quad (22)$$

The values of the coefficients related to this mathematical model have been taken from the real PCC in the Microgrid Laboratory of the University of Cuenca, details shown in Ref. [39].

4. Energy Management and Power Smoothing Techniques

4.1. Power Balance

The energy management performed by the controllers makes it possible to balance the power flow between sources and load. Considering the HRES of Figure 2, the boundary conditions are explained below:

$$P_t^L = \begin{cases} P_t^{REN} + P_t^{LI-} + P_t^{Gd,s}; \text{ If } P_t^{REN} \geq P_t^L \text{ and } \underline{SOC_t^{LI}} < SOC_t^{LI}(k) < \overline{SOC_t^{LI}} \\ P_t^{REN} + P_t^{Gd,s}; \text{ If } P_t^{REN} \geq P_t^L \text{ and } SOC_t^{LI}(k) \leq \underline{SOC_t^{LI}} \\ P_t^{LI-} + P_t^{Gd,b}; \text{ If } P_t^{REN} < P_t^L \text{ and } \underline{SOC_t^{LI}} < SOC_t^{LI}(k) < \overline{SOC_t^{LI}} \\ P_t^{Gd,b}; \text{ If } P_t^{REN} < P_t^L \text{ and } SOC_t^{LI}(k) \leq \underline{SOC_t^{LI}} \end{cases} ; \forall t \in T \cup \Xi \quad (23)$$

$$P_t^{REN} = P_t^{PV} + P_t^{HKT} + P_t^{WT} \quad (24)$$

The power smoothing methods generate the reference power signal that the SC will use to smooth the peaks. Figure 4 explains a basic diagram of power smoothing control using the SC for the proposed system that included P_t^{REN}. The electrical power in the SC is expressed with Equation (25) [43]. The reference power signal $\left(P_t^{ref}\right)$ will be generated by each method separately, i.e., output power of the ramp rated (RR) and moving average (MA) power smoothing method (P_t^{RR} and P_t^{MA}) respectively.

$$P_t^{SC} = \begin{cases} P_t^{ref} - P_t^{REN} \text{ if } \frac{d(P_t^{REN})}{dt} \geq r_{max} & ; \forall t \in T \cup \Xi \\ P_t^{REN} \text{ if } \frac{d(P_t^{REN})}{dt} < r_{max} & ; \forall t \in T \cup \Xi \end{cases} \quad (25)$$

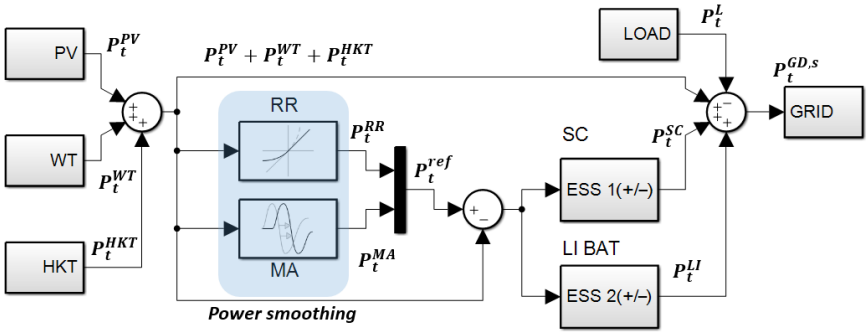

Figure 4. Control diagram of the power smoothing method by ramp rate control.

4.2. Ramp Rate

The ramp-rate control considers a maximum permissible ramp value of the power injected into the grid, r_{max} (%/min) if the power variation does not exceed r_{max}. The inverter injects all the available power from renewable sources. The control is activated when the maximum allowable ramp condition is broken, as expressed in Equation (26) [44]:

$$\left|\Delta(P_{t,\,min}^{REN})\right| > r_{max}; \forall t \in T \cup \Xi \quad (26)$$

To determine the parameter r_{max}, exhaustive tests were carried out for a year, from which we deduced that its average value is approximately r_{max}= 10%/min for the renewable sources [5]. The power fluctuation for a time (t) is calculated with Equation (27):

$$P_t^{RR} = \frac{|P(t) - P(t - \Delta t)|}{P^*} \times 100\%, \forall t \in T \cup \Xi \quad (27)$$

where P^* is the inverter power. If $(\text{abs}\left|\Delta P^{\Delta t}(t)\right| > r)$, the SC charging $(P_t^{SC} < 0)$ or discharging $(P_t^{SC} > 0)$ depend on the power ramp value [44].

4.3. Moving Average (MA)

The Moving Average (MA) algorithm is generally used in many power smoothing applications. The power sent to the grid is produced after measuring the power produced

by the PV system in a sampling time T_{sample} and then calculating an average value of k samples. This process is followed for each sampling time. The P_t^{SMA} reference value is calculated with Equation (28) [45]:

$$P_t^{MA} = SMA^i(P_t^{RES}); \forall t \in T \cup \Xi \quad (28)$$

where

$$SMA^i\left(P_t^{RES}\right) = \frac{\sum_{j=0}^{k-1}(P_t^{RES})_{j-1}}{k} \ (k \leq i); \ i = \frac{t}{T_{sample}}; \forall t \in T \cup \Xi \quad (29)$$

5. Results

This section presents and discusses various numerical results. The results were obtained from an experimental setup, which is described below and is based on real data. Moreover, various sensitivity analyses were performed with respect to various technical and economic indices.

5.1. Power Smoothing Results

In this stage, using the microgrid laboratory of the University of Cuenca, power smoothing tests were performed based on the mathematical models explained in the previous section. Figure 5 shows a pictographic representation of the equipment used in this experiment. The main parameters of the equipment are shown in Table 1 [39]. The Energy Management System (EMS) proposed in the experimental phase controls the variables from the SCADA system which is executed remotely through the Modbus TCP/IP communication protocol from the LabVIEW software. In parallel, through the same protocol, the reading, processing, and writing of variables are executed through a MATLAB script. In this way, a very fast processing and response time is obtained in the order of milliseconds. The reading parameters from the electrical grid are registered from the API network analyzers also linked to the SCADA system.

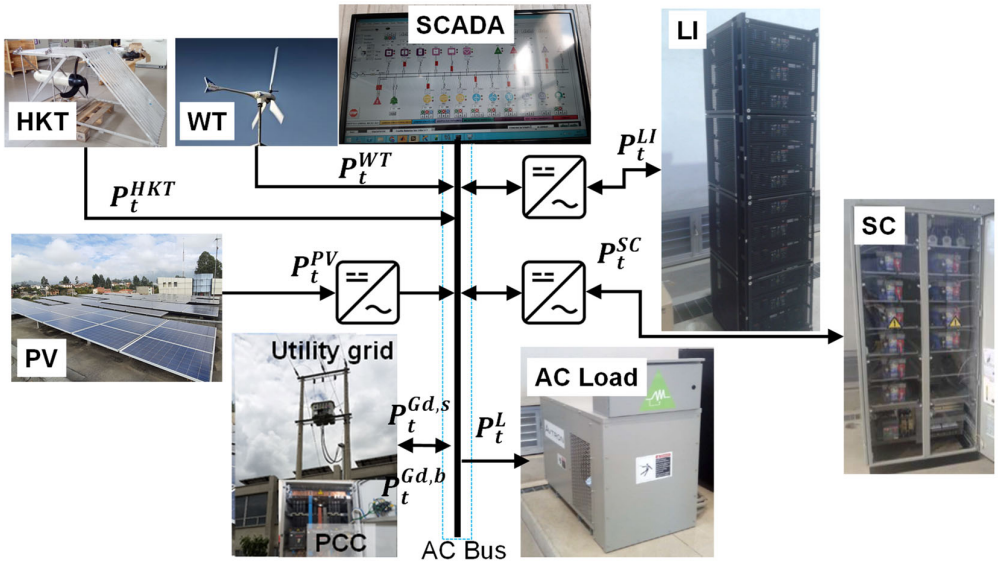

Figure 5. Connection diagram of the laboratory equipment used in this experiment.

Table 1. Technical characteristics of the microgrid laboratory equipment at the University of Cuenca [39].

Component	HKT	SC	Converter	PV	WT	LI
Type	Smart hydro	Maxwell	MG5KTL	Polycrystalline	E70 Pro Enair	Samsung
Specification	5 kW	56 V 130 F	50 kW	250 Wp	5 kW	44 kWh 642 V
Size	each unit	Variable	each unit	each unit	each unit	Variable

5.1.1. Configuration 1

The evaluation of power smoothing methods was conducted gradually, i.e., initially a basic system with a single renewable source (PV) and SC connected to the grid was analyzed. Figure 6 shows the control scheme of the first basic system. In this case, $P_t^{RES} = P_t^{PV}$ and $P_t^{ref} = P_t^{RES} - P_t^{RR}$ or $P_t^{ref} = P_t^{RES} - P_t^{MA}$.

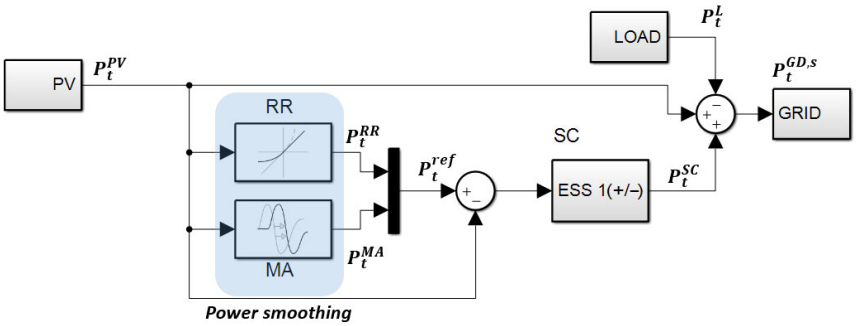

Figure 6. Control diagram, power smoothing methods for a system (PV + SC).

The response of the algorithm is observed in Figure 7, where the state of the smoothed power is compared when applying the RR and MA method. As observed in this figure, it is possible to mitigate the value of fluctuations. However, the demand curve shifts with respect to solar irradiance. This behavior could cause an oversizing of the PV system.

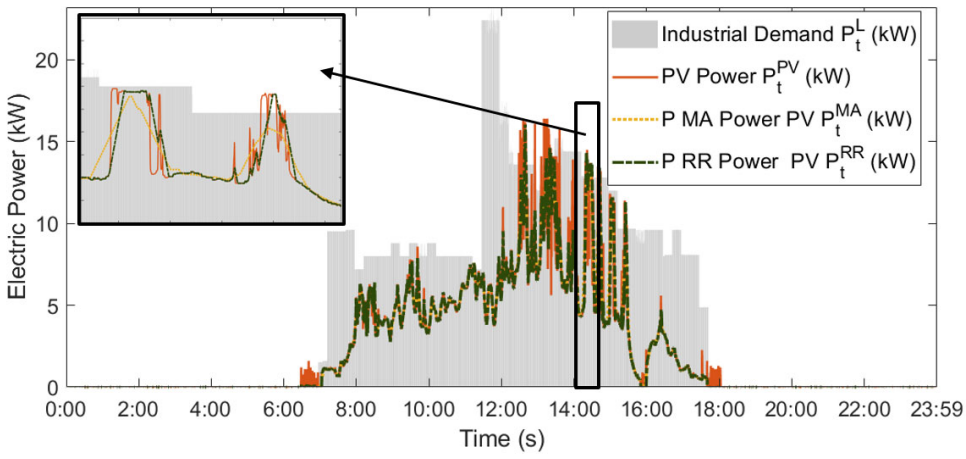

Figure 7. Control algorithm response, power smoothing methods for a system (PV + SC).

The main difference between the proposed power smoothing algorithms is based on the SC operability. Figure 8 shows the behavior of an SC with respect to fluctuations in PV power and load. In this sense, the use of an SC is compared when applying the two methods, RR and MA, for one day. The RR method established a range of 200 accumulated charge and discharge cycles, while MA was established in the range of 700 accumulated cycles. In another aspect, it was observed that the MA method forces the SC to operate on certain intervals unnecessarily.

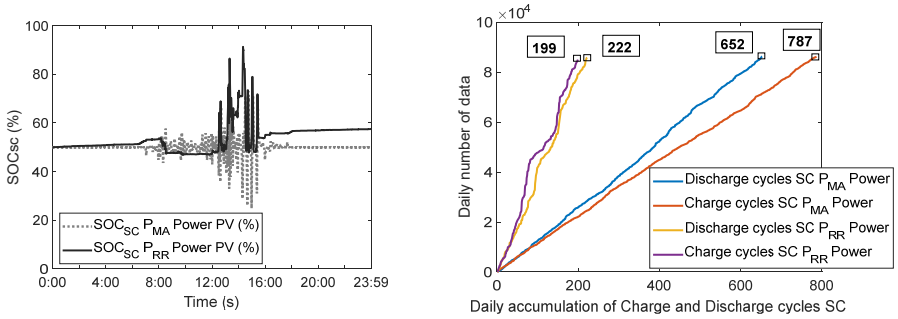

(**a**) (**b**)

Figure 8. SC operability in Configuration 1, time step one second: (**a**) state of charge; (**b**) cumulative charging/discharging cycles.

5.1.2. Configuration 2

For this new configuration, $P_t^{RES} = P_t^{PV} + P_t^{WT}$. Figure 9 shows the control diagram where the two proposed power smoothing methods are evaluated. The new reference powers include the wind component, $P_t^{ref} = P_t^{RES} - P_t^{RR}$ or $P_t^{ref} = P_t^{RES} - P_t^{MA}$.

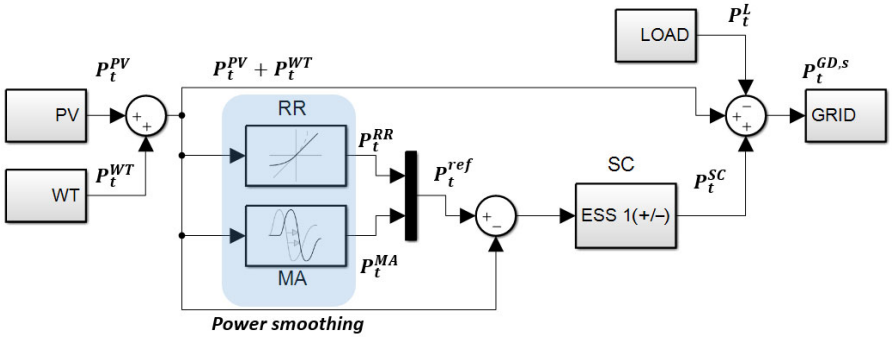

Figure 9. Control diagram, power smoothing methods for a system (PV + WT + SC).

The result seems evident; however, some peaks produced by the WT together with the PV system and the demand cause greater fluctuations in the system. Figure 10 shows that the power smoothing methods flatten the curve. It is important to mention that during 7:00 a.m. and 10:00 a.m., renewable sources do not supply the demand. In this case, the energy comes from the grid, reducing self-consumption.

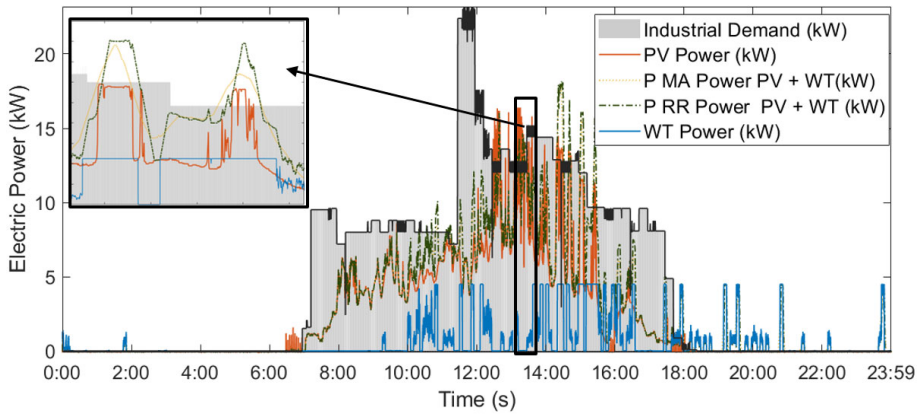

Figure 10. Control algorithm result, power smoothing methods for a system (PV + WT + SC).

Figure 11 shows the operation of the SC for Configuration 2. The RR method establishes a range of 300 charge and discharge cycles accumulated for one day, while MA is established in the range of 700 cycles. The coincidence of the PV and WT peaks causes power

ramps that exceed the minimum (10%/min) of the installed renewable capacity, causing an increase in the operability of the SC for the RR method with respect to Configuration 1, while the MA method keeps averaging the values.

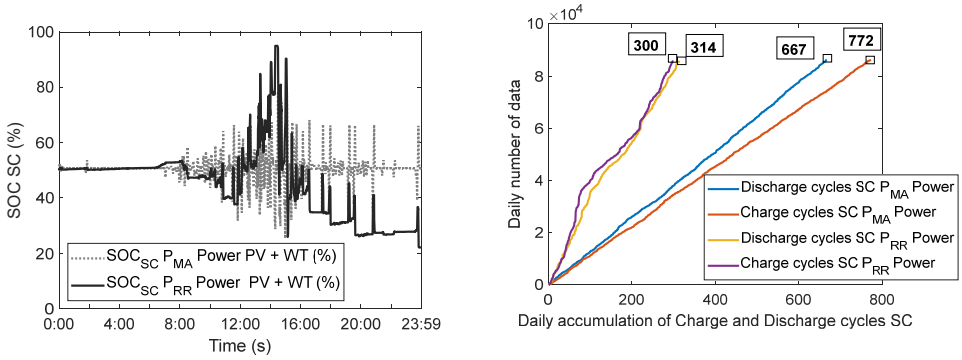

(**a**) (**b**)

Figure 11. SC operability in Configuration 2, time step one second: (**a**) state of charge; (**b**) cumulative charging/discharging cycles.

5.1.3. Configuration 3

Configuration 3 is shown in Figure 4. There is energy storage made up of lithium-ion batteries and hydrokinetic turbines; thus, $P_t^{RES} = P_t^{PV} + P_t^{WT} + P_t^{HKT}$. Therefore, $P_t^{ref} = P_t^{RES} - P_t^{RR}$ or $P_t^{ref} = P_t^{RES} - P_t^{MA}$.

Figure 12 shows the response of the algorithm; the HKT does not cause power peaks with ramps greater than 10%/min of the total renewable capacity. As it is not a dispatchable energy source, the energy generated will be used to supply the demand or recharge the batteries.

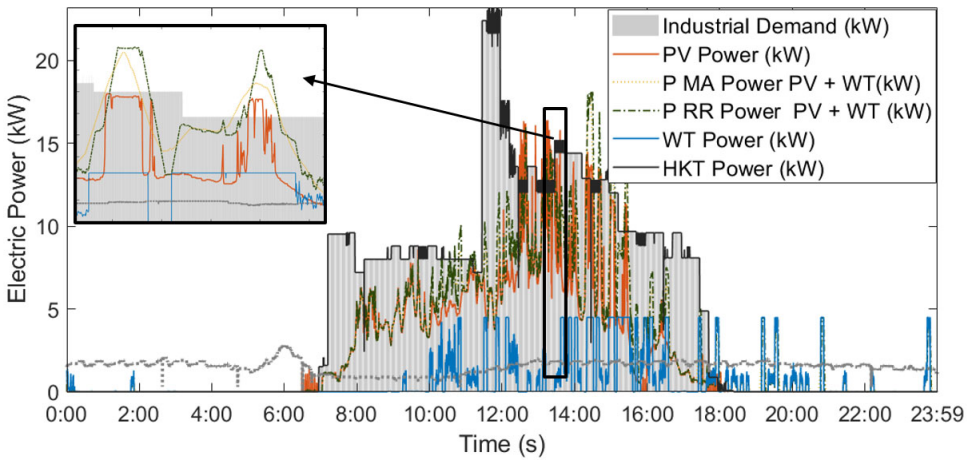

Figure 12. Control algorithm result, power smoothing methods for a system (PV + WT + HKT + LI + SC).

On the other hand, the LI battery does not participate in power smoothing. The operation of the SC is identical to Configuration 2. The state of charge of the LI battery and the SC is shown in Figure 13. The control algorithm discharges the LI battery when the conditions of the objective function are met, i.e., the renewable power is not enough to supply the demand. In contrast, LI is charged when there is surplus electricity. The SC performs power smoothing.

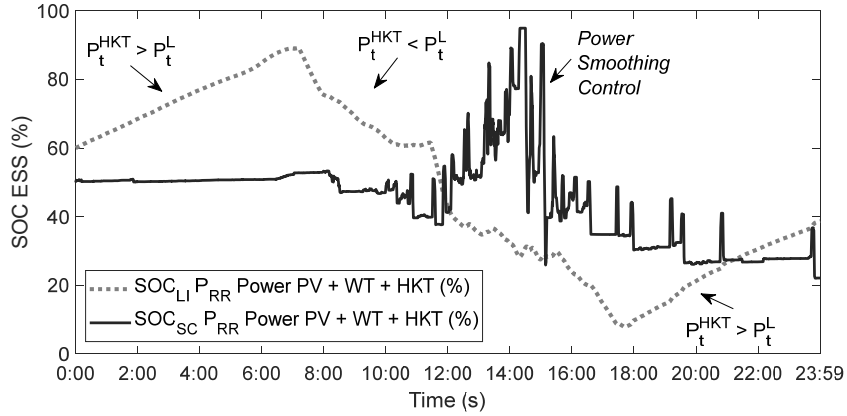

Figure 13. State of charge of the hybrid energy storage system for Configuration 3.

5.2. Energy Management Results

The uneven distribution of the RES profile causes a power imbalance. Table 2 shows the energy exchange between the HRES and the grid during a day with time steps of seconds. Clearly, renewable energy is not sufficient to supply demand using Configurations 1 and 2. However, Configuration 3 causes surplus electricity in the early morning hours, and throughout the rest of the day, electricity is purchased from the grid.

Table 2. Energy flow between the utility grid and HRES.

Configuration	To Grid (kWh/Day)	From Grid (kWh/Day)
1	52.99	59.55
2	62.64	49.9
3	151.91	26.63

5.3. Cost of Energy

In Ecuador, the energy cost for selling renewable energy to the grid can be considered on average 0.0658 USD/kWh [46] according to the Feed in Tariff (FIT) (Regulation No. CONELEC 001/13). Thus, the cost of energy for the industrial sector in Ecuador is considered to be 0.092 USD/kWh [47]. In this regard, the daily cost of exchanging HRES with the grid is shown in Table 3.

Table 3. Daily energy cost (the electricity tariff is considered fixed).

Configuration	To Grid (kWh/Day)	From Grid (kWh/Day)	Net (USD/Day)
1	3.49	5.48	−1.99
2	4.12	4.59	−0.47
3	10	2.45	7.55

The net gain for consumers does not consider capital costs. It is based on self-consumption. Configuration 3 produces more surplus electricity. It is important to mention that for this paper a 5 kW HKT, a 4.5 kW WT, and a 15 kW PV system have been considered.

5.4. Sensitivity Analysis

Sensitivity analysis studies the impact on a dependent variable of a model. Based on the defined capacities of the RES, this section presents the sensitivity analysis with respect to the capacity of (PV, WT, and HKT), analyzing the energy flow, self-consumption, and energy cost between the grid and HRES.

5.4.1. Case 1 (Base)

In this sense, Figure 14 presents the variation of the PV capacity with respect to the energy to/from the grid. In this case, an increase is established from 15 kWp to 40 kWp with steps of 5 kWp. It is evident that when increasing up to 35 kWp (that is, 133% of the base capacity), self-consumption is the maximum, and energy is not purchased from the grid, as shown in Table 4.

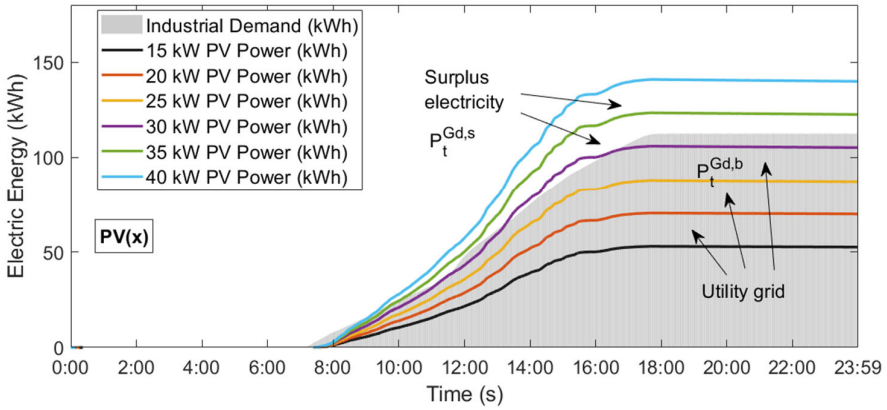

Figure 14. Sensitivity analysis with respect to PV capacity, Configuration 1.

Table 4. Daily energy cost and self-consumption for different PV capacities.

PV Capacity (kWp)	To Grid (USD/Day)	From Grid (USD/Day)	Net (USD/Day)	Self-Consumption (kWh/Day)
15	3.49	5.48	−1.99	−6.56
20	4.64	3.57	0.77	28.42
25	5.79	2.26	3.53	63.4
30	6.97	0.60	6.37	99.44
35	8.12	1.01	7.12	134.42
40	9.28	2.61	11.89	169.38

5.4.2. Case 2

A comparison is established to maintain PV generation and expand the WT (see Figure 15), with increased ranges from 4.5 kW per turbine to 27 kW which is 112.38% more than its base generation, where the system is self-sustaining and does not require energy from the grid. This means that the SC capacity must be doubled with respect to the base case.

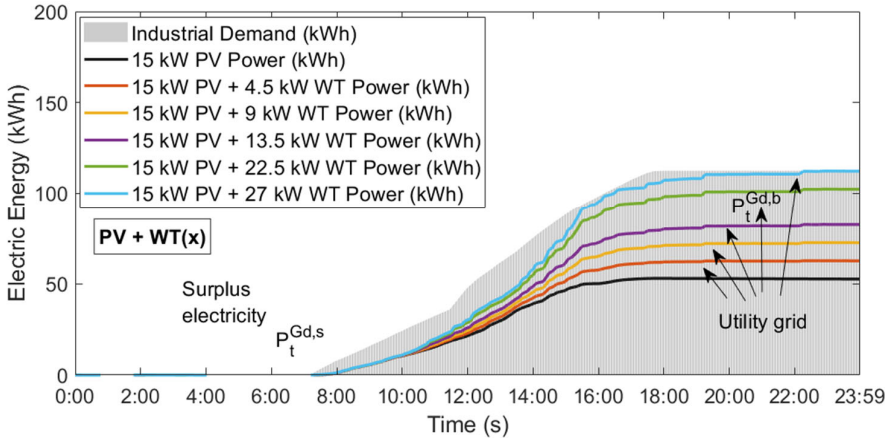

Figure 15. Sensitivity analysis with respect to WT capacity, Configuration 2.

Table 5 shows the increase in energy cost by expanding the WT capacity for Configuration 2. However, Case 1 (base) has 54.60% more profit than Case 2, and self-consumption is 60.9% higher.

Table 5. Daily energy cost and self-consumption for different WT capacities (PV = 15 kWp).

WT Capacity (kW)	To Grid (USD/Day)	From Grid (USD/Day)	Net (USD/Day)	Self-Consumption (kWh/Day)
0	3.49	5.48	−1.99	−6.56
4.5	4.12	4.59	−0.47	12.74
9	4.78	3.68	1.10	32.64
13.5	5.43	2.76	2.67	52.54
22.5	6.74	0.93	5.81	92.94
27	7.41	0	7.41	112.54

5.4.3. Case 3

When expanding the capacity of the HKT, the results shown in Figure 16 are obtained. Case 3 establishes a comparison to maintain PV generation and expand the HKT, with increased ranges of 5 kW per turbine. It is possible to balance renewable power and load demand up to 10 kW of the HKT capacity, i.e., 125.3% more than its current generation, which also implies keeping the current number of supercapacitors constant to mitigate the generated fluctuations. LI batteries are considered necessary to improve the system and balance demand with generation. In this case, the base capacity of an LI battery is 50 kWh.

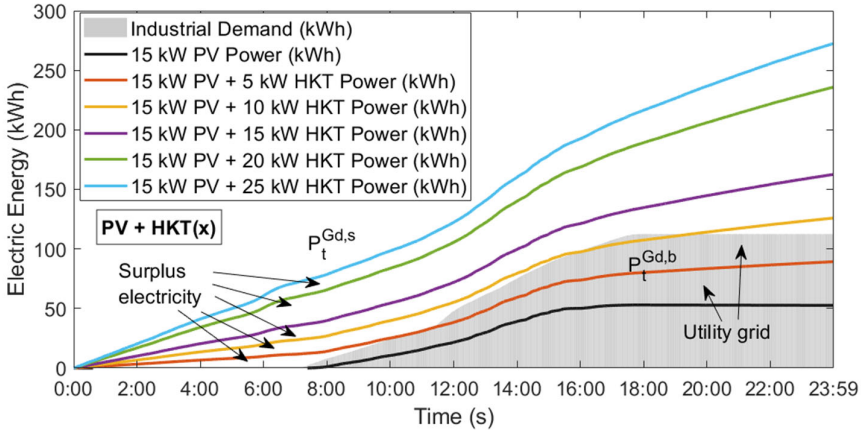

Figure 16. Sensitivity analysis with respect to the HKT capacity, PV = 15 kW, WT = 0 kW, and LI = 50 kWh.

The result in Table 6 shows that on average the increase in the HKT's capacity produces 83.2% and 46.2% of the energy cost and self-consumption with respect to the base case, respectively. The hydrokinetic resource contributes significantly to the sustainable improvement of the HRES.

Table 6. Daily energy cost and self-consumption for different HKT capacities (PV = 15 kWp).

HKT Capacity (kW)	To Grid (USD/Day)	From Grid (USD/Day)	Net (USD/Day)	Self-Consumption (kWh/Day)
0	3.49	5.48	−1.99	−6.56
5	5.87	2.14	3.73	66
10	8.28	−1.23	9.51	139.28
15	10.70	−4.60	15.30	212.6
20	15.52	−11.35	26.87	359.18
25	17.93	−14.62	32.65	432.48

5.4.4. Case 4

In Configuration 2, the WT capacity remains constant (4.5 kW) with respect to the increase in PV (x) as shown in Figure 17. Case 3 establishes a comparison to expand PV

generation and maintain the WT. The energy flow is balanced with PV = 30 kWp, i.e., 117.8% more than its base capacity, which also implies doubling the number of supercapacitors to mitigate fluctuations.

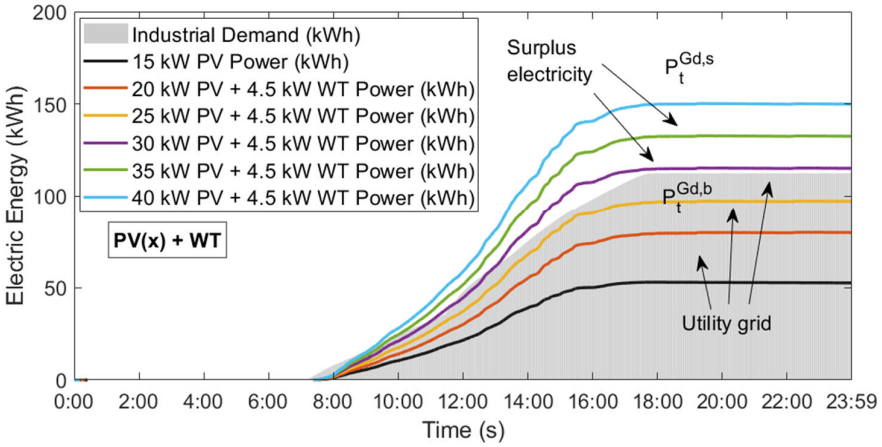

Figure 17. Sensitivity analysis with respect to PV capacity, Configuration 2.

The result shown in Table 7 differs with respect to Case 2. By increasing the PV capacity in Configuration 2, the energy cost and self-consumption are 63% and 19.27% higher with respect to the base case, respectively.

Table 7. Daily energy cost and self-consumption for different PV capacities (WT = 4.5 kW).

PV Capacity (kWp)	To Grid (USD/Day)	From Grid (USD/Day)	Net (USD/Day)	Self-Consumption (kWh/Day)
15	3.49	5.48	−1.99	−6.56
20	5.27	2.99	2.28	47.54
25	6.41	1.39	5.02	82.34
30	7.59	0.26	7.33	118.2
35	8.74	−1.87	10.61	153.12
40	9.89	−3.47	13.36	188.04

5.4.5. Case 5

Finally, Case 5 establishes a comparison to expand PV generation and maintain the HKT steps of 5 kW. As seen in Figure 18, it is possible to balance the demand and renewable generation with PV = 25 kW, which is 133.9% more than its base capacity. This also implies increasing (0.3 kW) the capacity of the base SC to mitigate the fluctuations generated. Likewise, the LI system is considered necessary to improve the system and balance demand with generation, with LI = 25 kWh.

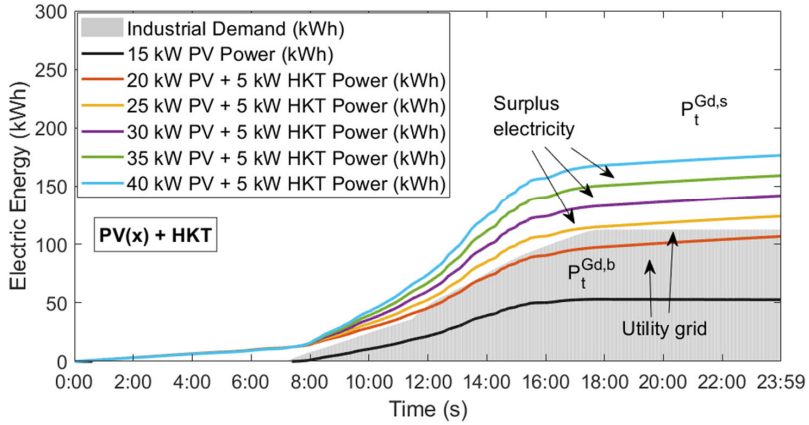

Figure 18. Sensitivity analysis with respect to PV capacity, HKT = 5 kW, WT = 0 kW, and LI = 50 kWh.

If the PV capacity is increased with respect to constant HKT, on average the energy cost is 58.3% higher than the base case, and there is a 73.4% increase in self-consumption. The energy and economic results are shown in Table 8.

Table 8. Daily energy cost and self-consumption for different PV capacities (HKT = 5 kW).

PV Capacity (kWp)	To Grid (USD/Day)	From Grid (USD/Day)	Net (USD/Day)	Self-Consumption (kWh/Day)
15	3.49	5.48	−1.99	−6.56
20	7.02	0.54	6.47	100.72
25	8.16	−1.05	9.21	135.44
30	9.34	−2.70	12.04	171.24
35	10.48	−4.30	14.78	205.96
40	11.62	−5.90	17.52	240.7

The summary of the results of the comparisons is presented in Figure 19. The optimal values are found in the demand generation balance line. The base case (PV + SC) requires all their electricity from the grid, while Case 5 sends high amounts of surplus electricity to the grid. When increasing the WT and PV generation, to expanding the SC capacity to smooth the peaks of power should be considered. If the capacity of the HKT and the LI battery is increased, the SC does not need to expand its capacity. Cases 2 and 3 present promising results regarding the energy balance between generation and demand with high levels of self-consumption.

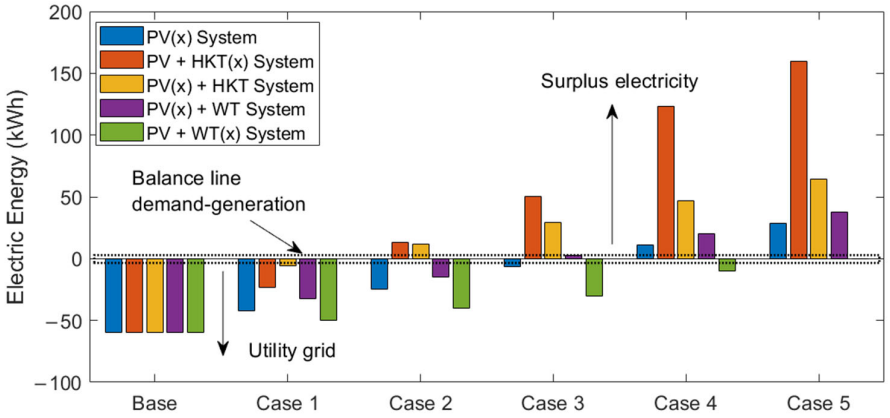

Figure 19. Energy exchange between HRES and the grid, sensitivity analysis of the proposed case studies.

The quantitative results are shown in Table 9. In this study, it is possible to analyze the optimal values required to supply the demand with an industrial profile expressed as follows: (i) The PV (x) case characterizes a progressive increase of the PV system up to 35 kW which must be doubled for the SC to increase its fluctuation ramps; (ii) The PV + HKT (x) case is an increase of 10 kW with HKT turbines that does not require expanding the storage capacity for SCs.

Table 9. Result of the sensitivity analysis regarding the capacity of renewable sources (x).

Cases	PV (kW)	WT (kW)	HKT (kW)	SC	LI
PV (x)	35	-	-	double	not required
PV + HKT (x)	15	-	10	single	double
PV (x) + HKT	25	-	5	double	single
PV (x) + WT	30	4.5	-	double	not required
PV + WT (x)	15	27	-	double	not required
PV + WT + HKT	15	4.5	5	single	single

However, to optimize and balance demand with generation, a robust LI system is required. (iii) The PV (x) + HKT case is an HKT and 25 kW in the PV system that is increased, which requires an increase for the SC similar to case (i) analyzed above. Additionally, it requires a low capacity of the LI battery system (50 kWh). (iv) The PV (x) + WT case increases a WT and 30 kW in the PV system, which requires an increase for the SC, similar to case (i) analyzed above. Similarly, compared to case (iii), it has less PV power but requires LI batteries. (v) The PV + WT (x) case progressively increases the WT up to 27 kW which requires an increase for the SC, similar to the cases above. It also does not require LI batteries. (vi) Finally, PV + WT + HKT is proposed, in which the PV system is maintained. The WT and HKT are increased. A combination of intermittent resources 15 kW and 4.5 kW maintain 5 kW combined with LI batteries that improve the performance of the system proposed in the study. The same is experimentally validated in the following subsection.

5.5. Voltage Response

One of the characteristics of the power smoothing methods to highlight is the voltage regulation in the PCC. Figure 20 shows the triphasic response for the base case. The parameters were taken from the microgrid laboratory supervisory control and data acquisition (SCADA) of the University of Cuenca. The nominal voltage of the utility grid is 120 Vac. Therefore, the result is within the parameters allowed by the electric company (5% for low-voltage industrial consumers) [48].

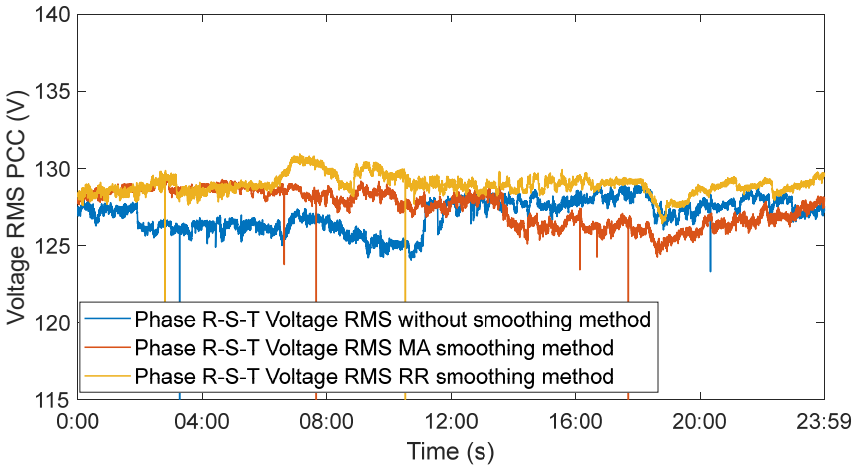

Figure 20. Voltage in alternating current bar, result when applying the proposed power smoothing methods, time window one day, resolution: hourly average data.

5.6. Model Accuracy

The accuracy of the model with respect to the simulations is shown in Figures 21 and 22. The results of the MA method shown in Figure 21 compare the simulated demand and that of the laboratory produced by a programmable load in AC. In addition, the results of the power smoothing method performed in Matlab based on the equations presented in this paper and the laboratory equipment are compared for the base case. It is evident that the simulated results present a better response due to the error when considering the response times of the SC and HKT, as well as the accuracy of the efficiency and cleanliness of the PV array during the simulation. However, the MA result with the laboratory equipment demonstrates the validity of the method to reduce fluctuations.

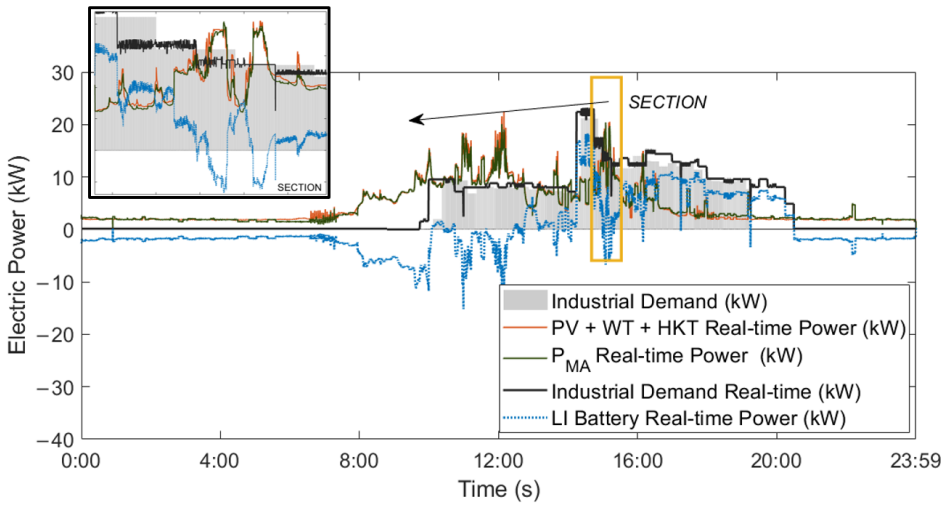

Figure 21. Comparison of the MA method between simulated data and laboratory tests.

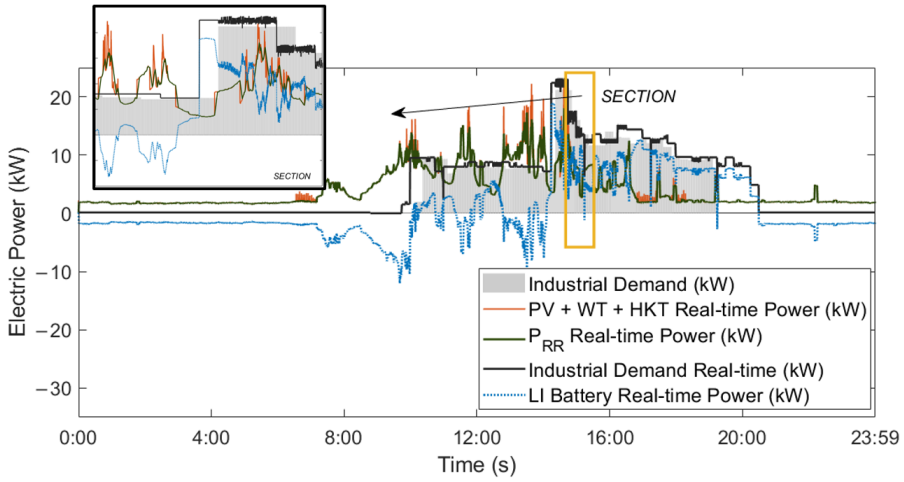

Figure 22. Comparison of the RR method between simulated data and laboratory tests.

In the same way, Figure 22 shows the results of the RR method through simulations in Matlab and laboratory tests (real data). This result presents better approximations with respect to the MA method, although the power curve slightly shifts from the PV output power, and the spikes are reduced. Clearly, the response of the equipment is similar to the computer simulation. The difference lies in the time constants of each source and the SC. For illustrative purposes, the annexes of the laboratory tests of the University of Cuenca are presented at the end of this document.

6. Conclusions

This paper presents a feasibility study of a renewable system connected to the grid, addressing various aspects based on energy quality and self-consumption. Two power smoothing algorithms (ramp rate and moving average) are presented for the combination of photovoltaic, wind turbine, and hydrokinetic turbine sources by means of supercapacitors. The results are based on technical and economic indices with experimental laboratory data in time step of seconds and are detailed below.

The main novelty of the proposed power smoothing algorithms is based on the operability of the supercapacitor. In Configuration 1, the ramp rate method establishes a range of 200 accumulated charging/discharging cycles/day of the supercapacitor, while the moving average remains in the range of 700 accumulated cycles. If a wind turbine capacity is increased, the ramp rate method establishes a range of 300 charge and dis-

charge cycles accumulated for one day, while the moving average remains in the range of 700 cycles. In summary, by increasing the wind source to hybrid renewable energy sources (photovoltaic + wind turbine), the supercapacitor operates 50% more times with respect to the photovoltaic system.

The sensitivity analyses with respect to capacity of RES for Case 1 (photovoltaic variable) show the viability to increase the photovoltaic capacity by 133% to reach self-sustainability, while the surplus electricity is sent to the grid.

The increase in intermittent photovoltaic and wind turbine resources requires expanding the fast response storage system such as the supercapacitor to mitigate the fluctuations generated. On the other hand, the increase in hydrokinetic turbine resources implies the use of ion lithium batteries as an energy reserve system for industrial demand. The proposed case photovoltaic, wind turbine, and hydrokinetic turbine is optimal for the dimensioning for storage systems. Using a supercapacitor improves voltage regulation at the point of common coupling during photovoltaic and wind turbine fluctuations.

The voltage at the point of common coupling resulting from the power smoothing methods is adjusted to the limits allowed by the electric company.

Finally, the results of the laboratory tests fit the simulations correctly. The errors produced are based on the constants of time, efficiency, and age of the renewable sources and supercapacitor.

Author Contributions: Conceptualization, D.B. and P.A.; data curation, D.B., P.A., M.T.-V. and A.E.; formal analysis, D.B., P.A., D.V., J.A.A. and F.J.; funding acquisition, M.T.-V. and F.J.; investigation, D.B. and P.A.; methodology, D.B., P.A., M.T.-V. and A.E.; project administration, M.T.-V., D.V., J.A.A. and F.J.; resources, D.V., A.E., J.A.A. and F.J.; software, D.V., A.E. and J.A.A.; supervision, D.V., J.A.A. and F.J.; validation, P.A., A.E. and F.J.; visualization, J.A.A. and F.J.; writing—original draft, D.B. and P.A.; writing—review and editing, M.T.-V., J.A.A. and F.J. All authors have read and agreed to the published version of the manuscript.

Funding: This research received no external funding.

Data Availability Statement: Not applicable.

Acknowledgments: The author (Paul Arévalo) thanks the Call for Grants for the Requalification of the Spanish University System for 2021–2023, Margarita Salas Grants for the training of young doctors awarded by the Ministry of Universities and financed by the European Union—NextGenerationEU. The authors thank Universidad de Cuenca for easing access to the facilities of the Microgrid Laboratory of the Centro Científico Tecnológico y de Investigación Balzay (CCTI-B), for allowing the use of its equipment, and for authorizing its staff the provision of technical support necessary to carry out the experiments described in this article. The icons used in this document were developed by Freepik, monkik, Smashicons and Pixel perfect, from www.flaticon.com (access 23 September 2022).

Conflicts of Interest: The authors declare no conflict of interest.

References

1. Sens, L.; Neuling, U.; Kaltschmitt, M. Capital expenditure and levelized cost of electricity of photovoltaic plants and wind turbines—Development by 2050. *Renew. Energy* **2021**, *185*, 525–537. [CrossRef]
2. Riffonneau, Y.; Bacha, S.; Barruel, F.; Ploix, S. Optimal Power Flow Management for Grid Connected PV Systems with Batteries. *IEEE Trans. Sustain. Energy* **2011**, *2*, 309–320. [CrossRef]
3. Saripalli, B.P.; Singh, G.; Singh, S. Supercapacitors based energy storage system for mitigating solar photovoltaic output power fluctuations. *World J. Eng.* **2022**. ahead of print. [CrossRef]
4. Lave, M.; Kleissl, J.; Arias-Castro, E. High-frequency irradiance fluctuations and geographic smoothing. *Sol. Energy* **2012**, *86*, 2190–2199. [CrossRef]
5. Ma, W.; Wang, W.; Wu, X.; Hu, R.; Tang, F.; Zhang, W.; Han, X.; Ding, L. Optimal Allocation of Hybrid Energy Storage Systems for Smoothing Photovoltaic Power Fluctuations Considering the Active Power Curtailment of Photovoltaic. *IEEE Access* **2019**, *7*, 74787–74799. [CrossRef]
6. Einan, M.; Torkaman, H.; Pourgholi, M. Optimized Fuzzy-Cuckoo Controller for Active Power Control of Battery Energy Storage System, Photovoltaic, Fuel Cell and Wind Turbine in an Isolated Micro-Grid. *Batteries* **2017**, *3*, 23. [CrossRef]
7. Amir, M.; Prajapati, A.K.; Refaat, S.S. Dynamic Performance Evaluation of Grid-Connected Hybrid Renewable Energy-Based Power Generation for Stability and Power Quality Enhancement in Smart Grid. *Front. Energy Res.* **2022**, *10*. [CrossRef]

8. Panhwar, I.H.; Ahmed, K.; Seyedmahmoudian, M.; Stojcevski, A.; Horan, B.; Mekhilef, S.; Aslam, A.; Asghar, M. Mitigating Power Fluctuations for Energy Storage in Wind Energy Conversion System Using Supercapacitors. *IEEE Access* **2020**, *8*, 189747–189760. [CrossRef]
9. Tostado-Véliz, M.; Arévalo, P.; Jurado, F. An optimization framework for planning wayside and on-board hybrid storage systems for tramway applications. *J. Energy Storage* **2021**, *43*, 103207. [CrossRef]
10. Wang, L.; Vo, Q.-S.; Prokhorov, A.V. Stability Improvement of a Multimachine Power System Connected with a Large-Scale Hybrid Wind-Photovoltaic Farm Using a Supercapacitor. *IEEE Trans. Ind. Appl.* **2017**, *54*, 50–60. [CrossRef]
11. Hashem, I.; Zhu, B. Metamodeling-based parametric optimization of a bio-inspired Savonius-type hydrokinetic turbine. *Renew. Energy* **2021**, *180*, 560–576. [CrossRef]
12. Shivashankar, S.; Mekhilef, S.; Mokhlis, H.; Karimi, M. Mitigating methods of power fluctuation of photovoltaic (PV) sources—A review. *Renew. Sustain. Energy Rev.* **2016**, *59*, 1170–1184. [CrossRef]
13. Hoff, T.E.; Perez, R. Modeling PV fleet output variability. *Sol. Energy* **2012**, *86*, 2177–2189. [CrossRef]
14. Datta, M.; Senjyu, T.; Yona, A.; Funabashi, T.; Kim, C.-H. A Frequency-Control Approach by Photovoltaic Generator in a PV–Diesel Hybrid Power System. *IEEE Trans. Energy Convers.* **2010**, *26*, 559–571. [CrossRef]
15. Datta, M.; Senjyu, T.; Yona, A.; Funabashi, T.; Kim, C.-H. A Coordinated Control Method for Leveling PV Output Power Fluctuations of PV–Diesel Hybrid Systems Connected to Isolated Power Utility. *IEEE Trans. Energy Convers.* **2009**, *24*, 153–162. [CrossRef]
16. Zarina, P.; Mishra, S.; Sekhar, P. Exploring frequency control capability of a PV system in a hybrid PV-rotating machine-without storage system. *Int. J. Electr. Power Energy Syst.* **2014**, *60*, 258–267. [CrossRef]
17. Lim, Y.S.; Tang, J.H. Experimental study on flicker emissions by photovoltaic systems on highly cloudy region: A case study in Malaysia. *Renew. Energy* **2014**, *64*, 61–70. [CrossRef]
18. Asif, A.A.; Singh, R. Further Cost Reduction of Battery Manufacturing. *Batteries* **2017**, *3*, 17. [CrossRef]
19. Wang, H.; Yao, C.-J.; Nie, H.-J.; Wang, K.-Z.; Zhong, Y.-W.; Chen, P.; Mei, S.; Zhang, Q. Recent progress in carbonyl-based organic polymers as promising electrode materials for lithium-ion batteries (LIBs). *J. Mater. Chem. A* **2020**, *8*, 11906–11922. [CrossRef]
20. García-Miguel, P.L.C.; Alonso-Martínez, J.; Gómez, S.A.; Plaza, M.G.; Asensio, A.P. A Review on the Degradation Implementation for the Operation of Battery Energy Storage Systems. *Batteries* **2022**, *8*, 110. [CrossRef]
21. Theuerkauf, D.; Swan, L. Characteristics of Open Circuit Voltage Relaxation in Lithium-Ion Batteries for the Purpose of State of Charge and State of Health Analysis. *Batteries* **2022**, *8*, 77. [CrossRef]
22. Alam, M.J.E.; Muttaqi, K.M.; Sutanto, D. Mitigation of Rooftop Solar PV Impacts and Evening Peak Support by Managing Available Capacity of Distributed Energy Storage Systems. *IEEE Trans. Power Syst.* **2013**, *28*, 3874–3884. [CrossRef]
23. Wang, S.; Tang, X.; Liu, X.; Xu, C. Research on Low Voltage Ride through Control of a Marine Photovoltaic Grid-Connected System Based on a Super Capacitor. *Energies* **2022**, *15*, 1020. [CrossRef]
24. Bharatee, A.; Ray, P.K.; Ghosh, A. A Power Management Scheme for Grid-connected PV Integrated with Hybrid Energy Storage System. *J. Mod. Power Syst. Clean Energy* **2022**, *10*, 954–963. [CrossRef]
25. Amine, H.M.; Mouaz, A.K.; Messaoud, H.; Othmane, A.; Saad, M. The impacts of control systems on hybrid energy storage systems in remote DC-Microgrid system: A comparative study between PI and super twisting sliding mode controllers. *J. Energy Storage* **2021**, *47*, 103586. [CrossRef]
26. Wang, K.B.; Xun, Q.; Zhang, Q. Recent progress in metal-organic frameworks as active materials for supercapacitors. *Energy Chem.* **2020**, *2*, 100025. [CrossRef]
27. Ma, W.; Wang, W.; Wu, X.; Hu, R.; Tang, F.; Zhang, W. Control Strategy of a Hybrid Energy Storage System to Smooth Photovoltaic Power Fluctuations Considering Photovoltaic Output Power Curtailment. *Sustainability* **2019**, *11*, 1324. [CrossRef]
28. Kamel, A.A.; Rezk, H.; Shehata, N.; Thomas, J. Energy Management of a DC Microgrid Composed of Photovoltaic/Fuel Cell/Battery/Supercapacitor Systems. *Electrochem. Capacit.* **2019**, *5*, 63. [CrossRef]
29. Foles, A.; Fialho, L.; Collares-Pereira, M.; Horta, P. An approach to implement photovoltaic self-consumption and ramp-rate control algorithm with a vanadium redox flow battery day-to-day forecast charging. *Sustain. Energy Grids Netw.* **2022**, *30*, 100626. [CrossRef]
30. Jiang, Y.; Fletcher, J.; Burr, P.; Hall, C.; Zheng, B.; Wang, D.-W.; Ouyang, Z.; Lennon, A. Suitability of representative electrochemical energy storage technologies for ramp-rate control of photovoltaic power. *J. Power Sources* **2018**, *384*, 396–407. [CrossRef]
31. Wu, T.; Yu, W.; Guo, L. A Study on Use of Hybrid Energy Storage System Along with Variable Filter Time Constant to Smooth DC Power Fluctuation in Microgrid. *IEEE Access* **2019**, *7*, 175377–175385. [CrossRef]
32. Abadi, S.A.G.K.; Bidram, A. A distributed rule-based power management strategy in a photovoltaic/hybrid energy storage based on an active compensation filtering technique. *IET Renew. Power Gener.* **2021**, *15*, 3688–3703. [CrossRef]
33. Masaki, M.S.; Zhang, L.; Xia, X. A hierarchical predictive control for supercapacitor-retrofitted grid-connected hybrid renewable systems. *Appl. Energy* **2019**, *242*, 393–402. [CrossRef]
34. Wang, G.; Ciobotaru, M.; Agelidis, V.G. Power Smoothing of Large Solar PV Plant Using Hybrid Energy Storage. *IEEE Trans. Sustain. Energy* **2014**, *5*, 834–842. [CrossRef]
35. Wang, L.; Vo, Q.-S.; Prokhorov, A.V. Dynamic Stability Analysis of a Hybrid Wave and Photovoltaic Power Generation System Integrated into a Distribution Power Grid. *IEEE Trans. Sustain. Energy* **2016**, *8*, 404–413. [CrossRef]

36. González, L.G.; Chacon, R.; Delgado, B.; Benavides, D.J.; Espinoza, J. Study of Energy Compensation Techniques in Photovoltaic Solar Systems with the Use of Supercapacitors in Low-Voltage Networks. *Energies* **2020**, *13*, 3755. [CrossRef]
37. Sukumar, S.; Marsadek, M.; Agileswari, K.; Mokhlis, H. Ramp-rate control smoothing methods to control output power fluctuations from solar photovoltaic (PV) sources—A review. *J. Energy Storage* **2018**, *20*, 218–229. [CrossRef]
38. Arévalo, P.; Cano, A.; Jurado, F. Comparative study of two new energy control systems based on PEMFC for a hybrid tramway in Ecuador. *Int. J. Hydrogen Energy* **2020**, *45*, 25357–25377. [CrossRef]
39. Espinoza, J.L.; Gonzalez, L.G.; Sempertegui, R. Micro grid laboratory as a tool for research on non-conventional energy sources in Ecuador. In Proceedings of the 2017 IEEE International Autumn Meeting on Power, Electronics and Computing ROPEC 2017, Ixtapa, Mexico, 8–10 November 2017; Institute of Electrical and Electronics Engineers Inc.: Piscataway, NJ, USA, 2017; pp. 1–7.
40. Arévalo, P.; Benavides, D.; Lata-García, J.; Jurado, F. Energy control and size optimization of a hybrid system (photovoltaic-hidrokinetic) using various storage technologies. *Sustain. Cities Soc.* **2019**, *52*, 101773. [CrossRef]
41. Kadri, A.; Marzougui, H.; Aouiti, A.; Bacha, F. Energy management and control strategy for a DFIG wind turbine/fuel cell hybrid system with super capacitor storage system. *Energy* **2019**, *192*, 116518. [CrossRef]
42. Wu, Y.; Long, X.; Lu, J.; Wu, Y.; Zhou, R.; Liu, L. Effect of temperature on the high-rate pulse charging of lithium-ion batteries. *J. Electroanal. Chem.* **2022**, *922*, 116773. [CrossRef]
43. De la Parra, I.; Marcos, J.; García, M.; Marroyo, L. Storage requirements for PV power ramp-rate control in a PV fleet. *Sol. Energy* **2015**, *118*, 426–440. [CrossRef]
44. Marcos, J.; Storkël, O.; Marroyo, L.; Garcia, M.; Lorenzo, E. Storage requirements for PV power ramp-rate control. *Sol. Energy* **2014**, *99*, 28–35. [CrossRef]
45. Atif, A.; Khalid, M. Saviztky–Golay Filtering for Solar Power Smoothing and Ramp Rate Reduction Based on Controlled Battery Energy Storage. *IEEE Access* **2020**, *8*, 33806–33817. [CrossRef]
46. Cobos, N.G.J.; Avecillas, F.Z.R.; Roldan, C.A.I.; Abad, J.L.E. Impacts on the consumption of electric power by the use of efficient refrigerators—Ecuador case. *Ingenius* **2017**, *18*, 53–63. [CrossRef]
47. ARCONEL. Tariff Schedule of the Electric Power Public Service for Ecuador. Resolution ARCERNNR-009. 2022. Available online: https://www.controlrecursosyenergia.gob.ec/wp-content/uploads/downloads/2022/05/Resolucion-ARCERNNR-009-2022.pdf (accessed on 23 September 2022).
48. ARCONEL. Distribution and Commercialization of Electrical Energy. Regulation 004/18. 2018. Available online: https://www.regulacionelectrica.gob.ec/wp-content/uploads/downloads/2018/11/arconel-004-18distribucion-y-comercializacion-de-energia.pdf (accessed on 20 March 2022).